Published in final edited form as:

Biochim Biophys Acta Biomembr. 2018 September ; 1860(9): 1670–1680. doi:10.1016/j.bbamem.2018.03.008.

The on-fibrillation-pathway membrane content leakage and off-fibrillation-pathway lipid mixing induced by 40-residue β-amyloid peptides in biologically relevant model liposomes☆

Qinghui Cheng, **Zhi-Wen Hu**, **Katelynne E. Doherty**, **Yuto J. Tobin-Miyaji**, **Wei Qiang***

Department of Chemistry, State University of New York at Binghamton, Binghamton, NY 13902, United States

Abstract

Disruption of the synaptic plasma membrane (SPM) induced by the aggregation of β-amyloid (Aβ) peptides has been considered as a potential mechanism for the neurotoxicity of Aβ in Alzheimer's disease (AD). However, the molecular basis of such membrane disruption process remains unclear, mainly because of the severe systematic heterogeneity problem that prevents the high-resolution studies. Our previous studies using a two-component phosphatidylcholine (PC)/phosphatidylglycerol (PG) model liposome showed the presence of Aβ-induced membrane disruptions that were either on the pathway or off the pathway of fibril formation. The present study focuses on a more biologically relevant model membrane with compositions that mimic the outer leaflet of SPMs. The main findings are: (1) the two competing membrane disruption effects discovered in PC/PG liposomes and their general peptide-to-lipid-molar-ratio dependence persist in the more complicated membrane models; (2) the SPM-mimic membrane promotes the formation of certain "on-fibrillation-pathway" intermediates with higher α-helical structural population, which lead to more rapid and significant of membrane content leakage; (3) although the "on-fibrillation-pathway" intermediate structures show dependence on membrane compositions, there seems to be a common final fibril structure grown from different liposomes, suggesting that there may be a predominant fibril structure for 40-residue Aβ (i.e. Aβ40) peptides in biologically-relevant membranes. This article is part of a Special Issue entitled: Protein Aggregation and Misfolding at the Cell Membrane Interface edited by Ayyalusamy Ramamoorthy.

Keywords

β-Amyloid peptides; Membrane disruption; Fibrillation; Solid-state nuclear magnetic resonance; spectroscopy

☆This article is part of a Special Issue entitled: Protein Aggregation and Misfolding at the Cell Membrane Interface edited by Ayyalusamy Ramamoorthy.

*Corresponding author. wqiang@binghamton.edu (W. Qiang).

Transparency document

The http://dx.doi.org/10.1016/j.bbamem.2018.03.008 associated with this article can be found, in online version.

Appendix A. Supplementary data

Supplementary data to this article can be found online at https://doi.org/10.1016/j.bbamem.2018.03.008.

1. Introduction

The main hypothesis for the pathology of Alzheimer's disease (AD), known as the amyloid cascade hypothesis (ACH), has been challenged over the past few years because of a number of current failures in the anti-amyloid drug developments [1–4]. Several types of drugs, including the active and/or passive antibodies for the β-amyloid (Aβ) aggregates and inhibitors for β/γ-secretases and co-factors, have shown only mild effects on the progression of the disease [2]. However, it is worth noting that some of these drugs, such as Bapineuzumab and Semagacestat, did reduce the production of Aβ or clear the existing Aβ plaques in early-phase clinic tests [3,5]. Therefore, it is prompt to address the question about the correlation between the aggregation of Aβ and the downstream consequences such as the disruption of neuronal cells, i.e. the molecular basis of the neurotoxicity of Aβ peptides.

Cellular membrane disruption induced by the aggregation of Aβ has been considered widely as a main neurotoxicity mechanism [6–9]. Particularly, the disruption of synaptic plasma membranes (SPMs) is thought to be highly biologically relevant, because the synaptic loss correlates strongly to the levels of cognitive decline and dementia in AD [10]. However, it remains a major challenge to understand the mechanistic details, and particularly the molecular basis, of the Aβ-induced membrane disruption because the model systems that are typically utilized for such mechanistic studies possess severe heterogeneity [11,12]. Aggregation of Aβ peptides may lead to the formation of multiple intermediates, which can be either on or off the pathway of fibrillation, and all intermediates may interact with membranes and result in multiple disruption pathways. The original ACH mainly focused on the fibrillation pathway, which may be insufficient to explain the neuronal toxicity. It has been recognized recently that the spherical Aβ oligomers, which are generally considered to be off the fibrillation pathway, might possess higher levels of neurotoxicity [13–18]. Therefore, such systematic heterogeneity can be biologically significant in the neurotoxicity mechanisms of Aβ. On the other hand, the heterogeneity also hinders the application of high resolution techniques such as the solid-state nuclear magnetic resonance (ssNMR) spectroscopy, which potentially serves as a highly suitable technique to probe the detailed molecular basis of Aβ aggregation and membrane interactions [19–21]. Therefore, it is necessary to reduce the heterogeneity so that individual membrane disruption effects can be studied in separated, well-controlled model systems.

There have been a large number of studies on the Aβ-induced membrane disruption mechanisms using model liposomes over the past decades [12,22]. Overall, these studies may be categorized by their approaches to generate model systems. The first category involves the addition of Aβ peptides into pre-formed liposomes, usually the large unilamellar vesicles (LUVs). In these studies, the peptides were usually treated before usage to remove any pre-existed large oligomers. Therefore, the initial states of Aβ peptides in these works could be considered as monomer or low-order oligomers. Fibrillation was typically reported in such systems when the initial Aβ concentrations were equal or higher than ~10 μM [23–28]. One recent single-molecular imaging study utilized sub-μM Aβ concentration and reported formation of small oligomers on membrane surfaces with restricted mobility, which might represent the nucleation step of Aβ in membrane-related environments [29]. A variety of membrane disruption effects have been observed in these

model systems, including the leakage of liposome content [23,30], changes in membrane curvatures [31], lipid uptake [32] and vesicle fusion [33,34]. There may be a mixture of several different membrane disruption effects in a particular system.

The second category of model systems are usually generated with pre-formed large Aβ oligomers in liposomes, where the initial peptide concentrations were higher than the previous model systems (i.e. ~100 μM or higher). These oligomers typically showed spherical morphologies on transmission electron microscopy (TEM) and were considered to be off the pathway of fibril formation [14,35]. A major membrane disruption mechanism that has been proposed in such model systems was the formation of cation-selected ion channels, which was supported by previous atomic force microscopy (AFM), the Black Lipids Membrane (BLM) assays and computational modeling [36–39]. It has been considered that the formation of ion channel might serve as a common mechanism in different types of amyloid diseases. In addition to the ion channel hypothesis, it has also been reported that large Aβ oligomers had the ability to fragmentize the lipid bilayers through detergent-like mechanisms, where the oligomeric cores were surrounded and stabilized by lipids [30,32]. Recently, it was suggested that the two processes might occur in steps, where the ion channels formed initially, and membrane fragmentation was induced at later stages. Changes in certain membrane compositions such as the gangliosides populations may trigger the membrane fragmentation process [32].

We have recently showed the reduction of systematic heterogeneity using simple model liposomes with only the zwitterionic lipid 1-palmitoyl-2-oleoyl-sn-glycerol-3-phosphocholine (POPC) and the negatively charged 1-palmitoyl-2-oleoyl-sn-glycerol-3-phosphoglycerol (POPG) and 40-residue Aβ (Aβ40) peptides [30]. Our results suggested three distinct membrane disruption effects, namely the leakage of liposome contents, the vesicle fusion and the membrane fragmentation, became predominant in individual model systems with well-controlled conditions. Our results indicated that the final structures of the Aβ40 aggregates in these three model systems were homogeneous and distinguishable to the resolution of ssNMR measurements, which suggested that the systematic heterogeneity of Aβ40-induced membrane disruption in POPC/POPG model liposomes could be reduced and the molecular basis (i.e. Aβ40-membrane interactions) in individual model systems could be studied in high-resolution details. Within these three distinct membrane disruption pathways, the first two involved addition of the Aβ40 peptides externally to liposomes, and the Aβ40-to-lipid molar ratio played key roles in shifting the predominance of liposome content leakage and lipid mixing [34].

This work describes an expansion of such systematic studies of the competition between fibrillation-induced membrane content leakage and non-fibrillation-induced lipid mixing in model liposomes with more biologically relevant membrane compositions. We prepared model liposomes with lipid compositions that mimic the outer leaflet of synaptic plasma membranes [40,41], where the major membrane interactions may occur when the peptides were released from the neuronal cells after enzymatic cleavage. Different events upon the external addition of Aβ40, such as the binding between peptides and membranes, the early-stage aggregation and membrane interactions, and the final-state Aβ40 structures, are investigated with systematic changes in the Aβ40-to-lipid molar ratios and membrane

compositions. Our results illustrate the distinct major membrane disruption effects that may occur both on and off the pathway of fibrillation with the externally added Aβ40 peptides. The biologically relevant membrane compositions, such as cholesterol, sphingomyelin and gangliosides, seem to have more significant influences on the initial binding and early-stage peptide conformation/membrane interactions rather than the final fibril structures.

2. Experimental section

2.1. Peptide synthesis and purification

All Aβ40 peptides, including the isotope-labeled and unlabeled sequences, were synthesized manually using routine Fmoc solid-phase peptide synthesis protocols. The crude products were cleaved from Valpre-loaded Wang resin using a mixture of trifluoroacetic acid/phenol/H_2O/1,2-ethanedithiol/thioanisole with volume ratio 9:0.5:1:0.5:0.25, purified using reversed-phase high-performance liquid chromatography (HPLC) with C18 reversed-phase columns, lyophilized and stored at −20 °C until usage. For all experiments described below, the peptides were freshly-dissolved in dimethyl sulfoxide (DMSO) and quantified using a nanodrop ultraviolet-visible (UV-VIS) spectrometer before the addition to pre-formed liposomes.

2.2. Liposome preparation

Three model liposomes were studied in this work, and their compositions were: (1) 1,2-dimyristoyl-*sn*-glycerol-3-phosphocholine(DMPC)/ 1,2-dimyristoyl-*sn*-glycerol-3-phospho-L-serine (DMPS)/cholesterol with 1.5:0.3:0.5 molar ratio; (2) DMPC/DMPS/sphingomyelin/cholesterol with 1.5:0.3:1.0:0.5 molar ratio; and (3) DMPC/DMPS/sphingomyelin/cholesterol/ganglioside GM1 with 1.5:0.3:1.0:0.5:0.15 molar ratio. For the fluorescence lipid mixing assay, liposomes were prepared with additional 0.5 mol% 1,2-dipalmitoyl-*sn*-glycerol-3-phosphoethnolamine-*N*-(7-nitro-21,3-benzoxadiazol-4-yl) (NBD-DPPE) and 1 mol% 1,2-dipalmitoyl-*sn*-glycerol-3-phosphoethnolamine-*N*-(lissamine rhodamine B sulfonyl) (Rh-DPPE) relative to the total lipids. All liposomes were prepared by mixing the lipid/cholesterol components in chloroform, followed by the formation of dried lipid film under N_2 flow and high-vacuum desiccator, 10 cycles of freeze-thaw in 10 mM phosphate buffer (pH 7.4 with 0.01% NaN_3) using liquid N_2 and 50 °C water-bath and 30 cycles of extrusion with 200 nm poresize membranes.

2.3. Analytical HPLC quantification of the binding of Aβ40 to membranes

A total 1.0 mL liposome solution was mixed with 20 μL Aβ40 stock solution in DMSO. The initial concentration of Aβ40 was kept at 10 μM for all HPLC quantifications and the Aβ40-to-lipid molar ratios varied from 1:30, 1:60, 1:90 to 1:120 for individual samples. For one set of measurements, the mixture was briefly vortexed for 5 min and the liposomes were pelleted down using ultracentrifugation (432,000 Xg for 30 min at 4 °C). For the other set of measurements, the mixture was vortexed and incubated quiescently at 37 °C for 4 h before ultracentrifugation. In both sets, supernatants were analyzed by HPLC with a reversed-phase C18 analytical-scale column and the linear H_2O-acetonitrile solvent gradient. The Aβ40 elution peaks were quantified based on the integrals from a standard working curve from freshly-dissolved Aβ40 in H_2O in the range of 0.5–10 μM.

2.4. Circular dichroism (CD) spectroscopy measurements

The CD measurements were applied on the re-suspended pellets from the ultracentrifugation described in the previous section (the HPLC quantification). The pellets (both with and without the 4-hour incubation) were re-suspended in 300 μL deionized H_2O, mixed thoroughly and loaded in a 0.1 cm Quartz CD cuvette. All spectra were collected at 20 °C and signal-averaged for 30 scans on a JASCO J-820 spectrophotometer, with the wavelength range 190–260 nm. All spectra were analyzed using CDPro package with the calibrated Aβ40 concentrations from the previous HPLC measurements (i.e. $[A\beta40]_{pellet} = 10\ \mu M - [A\beta40]_{supernatant}$).

2.5. Fluorescence kinetics assays

We applied three different fluorescence kinetics measurements, the calcein leakage assay, the thioflavin-T fibrillation assay and the lipid mixing assay, to investigate the kinetics of membrane content leakage, the Aβ40 fibrillation and the vesicle fusion, respectively. The procedures and experimental details, such as the excitation and emission wavelengths and slits, have been described in details in our previous studies [30,34]. For the current work, each individual assay was applied to a group of 12 samples with a combination of 4 peptide-to-lipid molar ratios and 3 membrane compositions. All measurements were performed within a 4-hour quiescent incubation time period, which was consistent with the timescale used for HPLC quantification and CD analysis. For each measurement, a background fluorescence signal was collected and subtracted from the raw kinetic curve of the corresponding sample. A circulating water-bath was utilized to maintain a stable temperature at 37 ± 3 °C during the measurements.

2.6. TEM imaging

The TEM images were collected for Aβ40-liposome samples with the peptide-to-lipid ratios 1:30 and 1:120, and with 4-hour and 7-day incubation time periods. All TEM samples were negatively stained with 2% uranyl acetate for ~30 s. The sample preparation for TEM imaging and instrument conditions have been provided in previous works [25].

2.7. Solid-state NMR spectroscopy

The ssNMR measurements were performed on a Bruker 600 MHz spectrometer installed with a 2.5 mm triple-resonance magic-angle-spinning (MAS) probe. All Aβ40-liposome samples utilized for ssNMR experiments were incubated at 37 °C for at least one week before ultracentrifugation. The pellets were lyophilized, packed into MAS rotors and re-hydrated before measurements. The sample temperature was kept at ~5–10 °C using cooling N_2 and monitored throughout the experiments based on the H_2O ^1H chemical shifts. TEM imaging was applied before and after the ssNMR measurements to ensure that fibril morphologies were not changed (Fig. S1 in Supporting information).

The two-dimensional (2D) ^{13}C-^{13}C spin-diffusion spectra were collected with radiofrequency-assisted diffusion (RAD) pulse sequence [42,43], starting from a 90 kHz ^1H $\pi/2$ pulse and a cross-polarization (CP) between ^1H and ^{13}C with ~60 kHz ^1H radiofrequency (*rf*) and ~50 kHz ^{13}C *rf* field and 30% linear ramp on ^{13}C. The spin-diffusion time periods were set to be 20 ms to observe intra-residue cross peaks only. A 10 kHz MAS

frequency was utilized for all measurements. The 2D spectra with short mixing time were collected in 12–24 h.

The ^{13}C-^{15}N frequency-selective rotational-echo double-resonance (fsREDOR) experiment [44] was done with the same initial ^{1}H π/2 pulse and CP conditions, followed by rotor-synchronized 50 kHz π-pulse trains in the ^{13}C channel and alternatively in the ^{15}N channel. The 1 ms frequency-selective Gaussian pulses were applied in the middle of π-pulse trains with the ^{13}C carrier frequency set on the Cγ of D23 and the ^{15}N carrier frequency set on the Nζ of K28. A 5 kHz MAS frequency was applied. The signal was collected with pulsed-spin locking (PSL) sequence [45] to achieve signal enhancement, using the PSL parameters described in literature. Each REDOR dataset 5 different dipolar evolution times from 1.6 ms to 14.4 ms was obtained in 24 h.

The ^{13}C constant-time PITHIRDs [46] experiments were performed on selectively-labeled Aβ40 sequences with ^{13}C isotope labeling on V18-CO and M35-CO. The MAS frequency was set to be 20 kHz and a 33 kHz π-pulse train (i.e. ~16.7 μs π pulses and 1/3 of the rotor period) was applied. The PSL acquisition was utilized with the ^{13}C carrier frequency set to ~174 ppm for the carbonyl carbons. Each PITHIRDs dipolar dephasing curve containing 8 dipolar evolution time from 0 to 33.6 ms was obtained within 24 h.

3. Results and discussion

3.1. Initial binding of Aβ40 to liposomes and the Aβ40-to-lipid-ratiodependence

We first quantified the binding between Aβ40 and membranes using analytical HPLC with and without the 4-hour incubation time periods. The same incubation time periods were utilized in our previous studies in the single-component POPC liposomes and the two-component POPC/POPG liposomes [30]. The percentages of binding shown in Fig. 1B were obtained based on the standard curve in Fig. 1A generated with freshly-dissolved Aβ40 peptides. Fig. 1B showed the plots of percentages for the most complicated membrane mimics that contained DMPC/PS/cholesterol/sphingomyelin/GM1, and additional results from other membrane compositions were summarized in Table S1 (in Supporting information). The results showed that there was little dependence of the binding percentages on the membrane composition. In addition, the current results were also consistent quantitatively with our previous analysis in POPC/POPG liposomes [30]. Initial binding (without incubation) percentages showed strong dependence on the Aβ40-to-lipid ratio, where increasing of the lipid abundance led to more rapid adsorption of Aβ40 peptides (i.e. the percentages were ~ 8%, 22%, 25% and 38% for the ratio 1:30, 1:60, 1:90 and 1:120 samples respectively). However interestingly, the increasing of binding percentages after 4-hour incubation showed less dependence on the Aβ40-to-lipid ratio. For instance, the percentage increased from 8% to 45% for 1:30 ratio sample, and for 1:120 samples the increment was from 38% to 75%. The increments for 1:60 and 1:90 samples were 40% and 42% respectively. In other words, a similar 40% additional absorption of Aβ40 peptides was observed within the 4-hour incubation, independent on the abundance of lipids. This observation suggested that the initial binding was likely to be caused by the adsorption of Aβ40 monomers or small oligomers to membranes, but this did not seem to be the predominant process of binding during incubation, because otherwise one would expect the

same dependence of binding percentage on Aβ40-to-lipid ratio before and after incubation. One possible explanation is that different types of nucleation (i.e. initial Aβ40 aggregates) were formed rapidly at the very early stage of binding. Therefore, the Aβ40 bound to these early-stage nuclei rather than membranes during incubation. The nucleus formed at higher ratio (e.g. 1:30) might have stronger ability to absorb monomeric peptides (i.e. stronger seeding effects) comparing to the one formed at lower ratio. Initial binding between Aβ40 monomer and membrane mimics that contained cholesterol, sphingomyelin and ganglioside GM1 have been studied extensively [47,48]. It was proposed that the clustered gangliosides increased the binding affinity of Aβ40 [49]. However, no significant difference in the population of bound Aβ40 was observed in our results for ganglioside-included and ganglioside-excluded membranes. This disagreement may relate to the major differences in lipid compositions, initial Aβ40 concentrations and pre-treatment of Aβ40 between our work and the published results [49].

3.2. Initial Aβ40 conformational changes

The structural changes within the first 4 h of incubation were studied using CD spectroscopy. Since all samples were pellet down with ultracentrifugation and the pellets were re-suspended for CD measurements, only membrane-bound Aβ40 peptides were analyzed. The raw CD spectra were analyzed to obtain the semi-quantitative distribution of secondary structures based on the membrane-bound Aβ40 concentrations determined by the HPLC analysis. The CD spectra were shown in Fig. 2A–F and the percentages of different secondary structures were plotted in Fig. 2G–H. Several conclusions can be drawn from the CD analysis. First, in all membrane types, there were large structured populations at the initial stage of binding of Aβ40 to membrane (Fig. 2A–C) but less structured populations after 4-hour incubation (Fig. 2D–F). Second, from the prediction of secondary structures, the α-helical population decreased and the β-strand/random coil populations increased within the 4-hour incubation time period. Such structural changes were also observed within a wide range of peptide-to-lipid molar ratio from 1:30 to 1:120. The observation supported a previous proposal where certain on-pathway α-helical intermediates of Aβ formed at the early stages of fibrillation in the presence of membranes [12]. It was suggested that membrane surface might catalyze the formation of such helical intermediates, which allowed Aβ to adopt an optimized orientation to facilitate further fibrillation. Third, the populations of α-helices at the initial stage of binding increased with the addition of sphingomyelin and ganglioside GM1 at any given Aβ40-tolipid ratio, suggesting that the initial binding conformations of Aβ40 were affected by the surface properties of membranes. It was known that the presence of sphingomyelin and cholesterol in membranes might promote the formation of micro-domains in lipid bilayers (i.e. lipid rafts) [50,51], and the addition of gangliosides might generate specific binding sites to Aβ peptides [52]. Both factors may contribute to the increasing in the helical population. Interestingly, the Aβ40 peptides adopted high populations of α-helices (i.e. 30%–45% depending on the Aβ40-to-lipid ratio) when they interacted with membranes that mimic the outer leaflets of synaptic vesicles. This result suggested that certain α-helical-enriched intermediates might be responsible for the early-stage synaptic disruption, because the in vivo concentrations of Aβ was likely to be much lower than the critical concentration of aggregation and therefore the on-pathway helical intermediates before aggregation might be dominant in biologically relevant

membrane environments. The presence of α-helical conformation upon the initial binding of Aβ40 to model membranes has been reported in literature. It was suggested that the preference of α-helical versus β-strand conformation was influenced by the relative ratio between Aβ40 and ganglioside GM1 [49,53]. Interestingly, the predicted populations in Fig. 2G showed the trend that the helical:strand ratio increased with the lipid:Aβ40 ratio (and therefore GM1:Aβ40 ratio), which was consistent in general with published works [49,53].

3.3. Thioflavin-T (ThT) fluorescence and TEM measurements on fibrillation

We next monitored the time-dependent ThT fluorescence emission intensities within the first few hours of incubation at 37 °C. Fig. 3A–C showed that in all membrane types, the ThT emissions increased immediately without lag periods, suggesting that the nucleation process was different in the presence of membranes comparing to the aqueous buffer, where a lag period was typically observed [54]. The membrane surface was likely to promote certain orientations of Aβ40 peptides that allowed immediate binding to ThT in a fluorescent-active configuration. All kinetic traces fit to single-exponential growth curve, and the rate constants were provided in Table 1. The rate constants roughly followed the trend of decreasing of Aβ40-to-lipid molar ratio, but with significant variations between different membrane compositions. In addition, the level of emission intensities decreased with the Aβ40-tolipid ratio in all membrane compositions. It is known that the ThT fluorescence intensity is sensitive to the molecular structures of Aβ aggregates [55]. The differences in ThT fluorescence intensities might be explained by distinct pathways of aggregation, which led to different aggregates. At high ratio such as 1:30, the initial aggregation led to higher population of β sheet structures and associated with higher level of ThT fluorescence; while at lower ratio, the aggregates contained lower population of ordered β sheets, and therefore disfavored the ThT binding. To test this possibility, we performed TEM imaging to the Aβ40-liposome systems with DMPC/DMPS/Cholesterol/sphingomyelin/ ganglioside GM1 and the Aβ40-to-lipid ratios 1:30 and 1:120 and 4-hour and 48-hour incubation time periods. Fig. 4 showed representative TEM images, which concluded that the formation of long Aβ40 fibrils were only observed at 1:30 Aβ40-to-lipid ratio with long-time incubation. The samples with 4-hour incubation showed mainly intact liposomes at both peptide-to-lipid ratios. Within long incubation time period, the sample with 1:120 ratio contained liposomes with surface-associated spherical species (i.e. indicated by arrows in Fig. 4C) but not fibrils. It was unclear whether these spherical species were actually bound to membrane surface or only attached to liposomes during TEM grid preparation. Noted that the initial Aβ40 concentrations were kept constant for both samples with 1:30 and 1:120 ratios, the absence of fibrillation at lower ratio was not because of absolute abundance of peptides, but the changes in relative abundance between peptides and lipids Overall, the results from our analytical HPLC, CD, ThT fluorescence and TEM measurements highlighted the significance of Aβ40-to-lipid molar ratio in alternating the peptide aggregation pathways. At higher ratio, the membrane-associated peptides formed an initial structure with high population of β-strand (more likely β sheets) during the first few hours of incubation, which promoted the ThT fluorescence and led to the final fibrillation. At lower ratio, on the other hand, the aggregation process did not lead to fibrillation (with lower growth of ThT fluorescence). The spherical species shown in Fig. 4C might represent certain off-fibrillation-pathway Aβ40 oligomers. Furthermore, our current and previous works

demonstrated similar effects of the Aβ40-to-lipid molar ratio on the aggregation pathways in a variety of membrane mimics including POPC, POPC/POPG, POPC/POPG/cholesterol, DMPC/DMPS/cholesterol, DMPC/DMPS/cholesterol/sphingomyelin and DMPC/DMPS/cholesterol/sphingomyelin/ganglioside GM1, strongly suggesting that the relative abundance of Aβ40 peptides to the total lipids in biological membranes plays important roles in the peptides' aggregation process.

3.4. Monitoring the time-dependent membrane leakage and lipid mixing

We next investigated the potential membrane disruption effects caused by the early-stage aggregation of Aβ40 with liposomes. Our CD data (Fig. 2) suggested that the promotion of α-helices within the first 4-hour incubation time periods upon the addition of sphingomyelin and ganglioside GM1. Using the well-developed calcein vesicle leakage and lipid mixing fluorescence assays [30], we studied the possible corresponding membrane disruption effects. Fig. 5 showed the calcein leakage and lipid mixing kinetic traces with various membrane components and Aβ40-to-lipid molar ratios. Each curve was fit to a singleexponential growth $I(t) = I_0 + I_1(1 - \exp(-kt))$, and Tables 1–2 summarize the best-fit rate constants k and the levels of membrane disruption, which were quantified as $(I_0 + I_1)/I_{max}$ with I_{max} represented the maximum membrane disruption obtained by adding 1% Triton X-100 to the liposomes. Table 2 (fitting for the calcein leakage assay) showed that the levels as well as the rates of Aβ40-induced membrane content leakage increased with the Aβ40-to-lipid ratio. Similar observations have been reported in our previous studies for POPC, POPC/POPG and POPC/POPG/cholesterol liposomes [30], and therefore illustrate a universal positive correlation between fibrillation and induced membrane content leakage. In other words, it is likely that membrane content leakage is caused by certain on-fibrillation-pathway intermediates of Aβ40 peptides.

Table 3 (fitting for the lipid mixing assay) summaries the levels and rates of induced lipid mixing. Opposite to the level of membrane leakage, the induced lipid mixing negatively correlated to the Aβ40-tolipid ratio, i.e. higher level of lipid mixing was observed at lower ratio. Similar trend has also been observed in our previous work in POPC and POPC/POPG membranes [34]. We have proposed that the competition between membrane content leakage and lipid mixing when changing the Aβ40-to-lipid ratio was led by the predominance of either Aβ40-Aβ40 or Aβ40-lipid interactions involving the same segments of peptides. It seems from the present work that such interactions are independent on membrane compositions. However, it is somewhat surprising that the rates of lipid mixing decrease with the ratio. For DMPC/DMPS/cholesterol and DMPC/DMPS/cholesterol/ganglioside membranes with Aβ40-to-lipid ratio 1:30, the maximum ~20% and ~5% lipid mixing was observed with relatively higher rates comparing to the samples with the same membrane compositions but lower ratios. The same phenomena were observed previously in POPC and POPC/POPG samples as well, where ~10% lipid mixing was induced at 1:30 ratio very rapidly. Future high-resolution studies on the early-stage Aβ40 intermediates in membrane environments may help to understand this observation. Additionally, the lipid mixing was eliminated in the DMPC/ DMPS/cholesterol/sphingomyelin/ganglioside GM1 sample with 1:30 ratio. Therefore, this particular model system may be used in the future to study the mechanisms of Aβ40-induced membrane content leakage and the resulted fibrillation.

3.5. Structural similarity in biologically relevant membrane mimics comparing with the POPC membrane

Given the fact that the addition of sphingomyelin and ganglioside GM1 did affect the initial Aβ40 conformation upon membrane binding, membrane leakage and lipid mixing, we then utilized ssNMR spectroscopy to investigate whether the Aβ40 fibril structures were different in the most biologically relevant membrane mimics comparing to the simplest POPC membranes. All fibrils were incubated for over a week and the ^{13}C isotope labeling was incorporated in selected residues. Fig. 6 showed the representative 2D ^{13}C-^{13}C spin diffusion spectra with 1D slices of Aβ40 fibrils in these two membranes (additional spectra shown in Supporting information). Three different labeled Aβ40 peptides were utilized, and the combined results covered residues L17, V18, F20, D23, S26, N27, K28, G29, A30, I32, G33, L34, G38 and V39. Table 4 summarizes the residue-specific ^{13}C chemical shifts for these two fibrils. To the solution of ssNMR spectroscopy, there were no obvious differences in residue-specific ^{13}C chemical shifts (also shown in the representative 1D slices). Variations within 0.5 ppm ^{13}C chemical shifts were attributed to the linewidths. Therefore, the second structures of fibrils do not seem to be affected by the membrane compositions.

To test the similarity of these two fibrils at the level of tertiary structures, we performed the ^{13}C-^{15}N frequency-selective rotational-echo double resonance (fsREDOR) and ^{13}C-PITHIRDs spectroscopy to detect the potential salt bridge interaction between D23 Cγ and K28 Nζ and the parallel-in-register β sheets, respectively. These measurements were done using selectively labeled Aβ40 fibrils. The absence of the D23 Cγ-K28 Nζ salt bridge in both fibrils was shown by ^{13}C-^{15}N fsREDOR in Fig. 7A. The D23 Cγ-K28 Nζ salt bridge was reported in a number of known Aβ fibril structures [56,57], but missing in some other cases [58–61], suggesting that this particular interaction might stabilize the hydrophobic core of fibrils, but not necessarily to drive the formation of fibril core. Finally, we employed ^{13}C-PITHIRDs-CT spectroscopy to confirm that the residues V18 and M35 were in the parallel-in-register β sheet segments in both Aβ40 fibrils (i.e. Fig. 7B–C). Overall, the ssNMR measurements supported that the Aβ40 fibrils grown in the biologically relevant membrane mimics and simple POPC membrane were very similar in terms of both secondary and tertiary structures.

3.6. Implication of the biophysical and structural studies

The combination of CD, Fluorescence, TEM and ssNMR results raise a possibility that changes in membrane compositions might only affect the very early stages of aggregation of Aβ40, while the final fibril structure is only determined by the structure of certain stable nuclei that are formed at the end of the early-stage structural conversions. The CD data at high Aβ40-to-lipid ratio showed that although the initial α-helical population enhanced with the addition of sphingomyelin and ganglioside GM1, the secondary structures of peptides after only a few hours incubation time period were in fact similar for different membrane compositions (and mostly random coils). This observation seems to suggest that certain non-helical early-stage conformations of Aβ40 must be achieved before the peptide can propagate into fibrils. Furthermore, it is worth noting the effects of Aβ40-to-lipid ratio on such early-stage structural conversions and the consequences on fibrillation. At higher ratio (e.g. 1:60 shown in Fig. 2C–D), the structural conversions showed higher tendency from α-

helices to β-strands within 4 h. In the meanwhile, there was a rapid increase in the ThT fluorescence, suggesting the formation of β-sheet structures. Although the TEM images did not show formation of fibrils or proto-fibrils during this short time period, the CD and ThT results suggested the formation of certain β-sheet-enriched small oligomers of Aβ40, which was on the pathway of fibrillation. Interestingly, our results suggested that the ThT fluorescence emission, which are routinely utilized as an indication of fibril formation, might not reflect quantitative fibril elongation kinetics in the presence of liposomes because certain early-stage aggregation process apparently led to strong ThT emission in the absence of fibrils. At lower ratio (e.g. 1:120 shown in Fig. 2C–D), the early-stage structural conversion showed lower tendency from α-helices to β-strands, but higher tendency from α-helices to random coils, and such process was accompanied by lower ThT fluorescence emissions within the 4hour incubation time period and the absence of amyloid fibrils after long incubation. It was likely that the higher relative abundance of lipids facilitated a distinct nucleation process, which produced Aβ40 oligomers off the pathway of fibrillation. Together with our previous studies in POPC, POPC/POPG and POPC/POPG/cholesterol vesicles, we have identified in a variety of model membranes that the main membrane disruption effects were influenced by the relative abundance of lipids to Aβ40 peptides. Fig. 5 showed that membrane content leakage occurred predominantly at higher Aβ40-to-lipid ratio and lipid mixing was the main disruption effect at lower ratio. Depending on the relative abundance of Aβ40 to the total lipids, the peptide aggregation process may take distinct pathways with different early-stage structural conversions, final products and the membrane disruption effects. Therefore, partial reduction of the Aβ40 concentrations and/or clearance of the existing amyloid plaques do not necessarily eliminate the neurotoxicity, which may explain the failures in recent anti-amyloid drug developments [2,3,23,62].

It is important to correlate the neurotoxicity of Aβ peptides to the structural information so that the molecular mechanisms of the Alzheimer's diseases can be understood in greater details. Our results suggested that the higher percentage of α-helices at the initial membrane-binding states of Aβ40 might correlate to more rapid membrane content leakage because the kinetics of leakage increased with the addition of sphingomyelin and ganglioside GM1 (i.e. Table 2) at the same Aβ40-to-lipid molar ratio. The detailed membrane interaction mechanisms of Aβ40 are associated with the early-stage structural conversions from α-helices to either β-strands or random coils, which may be affected by the lipid abundance. Therefore, future mechanistic studies will focus on two questions: First, what kinds of molecular interactions between Aβ40 and specific membrane components, potentially sphingomyelin and gangliosides GM1, promote the α-helical conformation? Second, what key early-stage structural conversions are responsible for the individual membrane disruptions (i.e. membrane content leakage and lipid mixing) at different Aβ40-to-lipid molar ratios? The presence of partially α-helical Aβ40 peptides has been considered as a universal early-stage folded state in aqueous solution, ganglioside-GM1-contained micelles and phosphatidylcholine vesicles. A recent solution NMR study demonstrated that the two potential segments that had high tendency to form helical conformation in membrane-bound Aβ40 were K16-G25 and I32-V36 [63]. These segments were also conserved membrane binding segments in previous works [16,63,64]. Interestingly, these segments have also overlapped with the typically β-sheet-enriched hydrophobic core regions

in known Aβ40 fibril structures. We have also previously shown that the segment around A21 was involved in the early stage structural changes in both on-fibrillation-pathway and off-fibrillation-pathway processes in samples with different Aβ40-tolipid ratios [26,34]. It is likely that the early-stage structural conversions in these segments lead to membrane disruptions.

Supplementary Material

Refer to Web version on PubMed Central for supplementary material.

Acknowledgements

This work is supported by the Startup Fund from Research Foundation of the State University of New York (910247–36), the National Science Foundation (NSF MRI 0822915) and the National Institutes of Health (GM125853). We appreciate the help from Dr. Juergen Schulte on ssNMR experiments.

References

[1]. Hardy JA, Higgins GA, Alzheimer's disease: the amyloid cascade hypothesis, Science 256 (5054) (1992) 184–185. [PubMed: 1566067]

[2]. Karran E, Mercken M, De Strooper B, The amyloid cascade hypothesis for Alzheimer's disease: an appraisal for the development of therapeutics, Nat. Rev 10 (2011) 698–712.

[3]. Tayeb HO, Murray ED, Price BH, Tarazi FI, Bapineuzumab and solanezumab for Alzheimer's disease: is the 'amyloid cascade hypothesis' still alive? Expert. Opin. Biol. Ther 13 (7) (2013) 1075–1084. [PubMed: 23574434]

[4]. Luo J, Warmlander SK, Graslund A, Abrahams J, Cross-interactions between the Alzheimer disease amyloid-b peptide and other amyloid proteins: a further aspect of the amyloid cascade hypothesis, J. Biol. Chem 291 (32) (2016) 16485–16493. [PubMed: 27325705]

[5]. Salloway S, Sperling R, Fox NC, et al., Two phase 3 trials of bapineuzumab in mild-to-moderate Alzheimer's disease, N. Engl. J. Med 370 (2014) 322–333. [PubMed: 24450891]

[6]. Yip CM, McLaurin J, Amyloid-beta peptide assembly: a critical step in fibrillogenesis and membrane disruption, Biophys. J 80 (2001) 1359–1371. [PubMed: 11222297]

[7]. Milanesi L, Sheynis T, Xue WF, Orlova EV, Hellewell AL, Jelinek R, Hewitt EW, Radford SE, Saibil HR, Direct three-dimensional visualization of membrane disruption by amyloid fibrils, Proc. Natl. Acad. Sci 109 (50) (2012) 20455–20460. [PubMed: 23184970]

[8]. Brender JR, Salamekh S, Ramamoorthy A, Membrane disruption and early events in the aggregation of the diabetes related peptide IAPP from a molecular perspective, Acc. Chem. Res 45 (3) (2012) 454–462. [PubMed: 21942864]

[9]. Walsh P, Vanderlee G, Yau J, Campeau J, Sim VL, Yip CM, Sharpe S, The mechanism of membrane disruption by cytotoxic amyloid oligomers formed by prion protein (106–126) is dependent on bilayer composition, J. Biol. Chem 289 (15) (2014) 10419–10430. [PubMed: 24554723]

[10]. Reddy PH, Beal MF, Amyloid beta, mitochondrial dysfunction and synaptic damage: implications for cognitive decline in aging and Alzheimer's disease, Trends Mol. Med 14 (2008) 45–53. [PubMed: 18218341]

[11]. Eckert GP, Wood WG, Mueller WE, Lipid membranes and beta-amyloid: a harmful connection, Curr. Protein Pept. Sci 11 (2010) 319–325. [PubMed: 20423299]

[12]. Butterfield SM, Lashuel HA, Amyloidogenic protein-membrane interactions: mechanistic insight from model systems, Angew. Chem 49 (2010) 5628–5654. [PubMed: 20623810]

[13]. Walsh DM, Klyubin I, Fadeeva JV, Cullen WK, Anwyl R, Wolfe MS, Rowan MJ, Selkoe DJ, Naturally secreted oligomers of amyloid beta protein inhibit hippocampal long-term potentiation in vivo, Nature 416 (6880) (2002) 535–539. [PubMed: 11932745]

[14]. Kayed R, Head E, Thompson JL, Mclntire TM, Milton SC, Cotman CW, Glabe CG, Common structure of soluble amyloid oligomers implies common mechanism of pathogenesis, Science 300 (5618) (2003) 486–489. [PubMed: 12702875]

[15]. Ahmed M, Davis J, Aucoin D, Sato T, Ahuja S, Aimoto S, Elliott JI, Van Nostrand WE, Smith SO, Structural conversion of neurotoxic amyloid-beta(1–42) oligomers to fibrils, Nat. Struct. Mol. Biol 17 (2010) 561–567. [PubMed: 20383142]

[16]. Yu X, Wang QM, Pan QF, Zhou FM, Zheng J, Molecular interactions of Alzheimer amyloid-beta oligomers with neutral and negatively charged lipid bilayers, Phys. Chem. Chem. Phys 15 (23) (2013) 8878–8889. [PubMed: 23493873]

[17]. Ferreira ST, Lourenco MV, Oliveira MM, De Felice FG, Soluble amyloid-beta oligomers as synaptotoxins leading to cognitive impairment in Alzheimer's disease, Front. Cell. Neurosci 9 (2015) 191. [PubMed: 26074767]

[18]. Ungureanu A, Benilova I, Krylychkina O, Braeken D, De Strooper B, Van Haesendonck C, Dotti CG, Bartic C, Amyloid beta oligomers induced neuronal elasticity changes in age-dependent manner: a force spectroscopy study on living hippocampal neurons, Sci. Rep 6 (2016) 25841. [PubMed: 27173984]

[19]. Tycko R, Molecular structure of amyloid fibrils: insights from solid-state NMR, Q. Rev. Biophys 39 (1) (2006) 1–55. [PubMed: 16772049]

[20]. McDermott A, Structure and dynamics of membrane proteins by magic angle spinning solid-state NMR, Annu. Rev. Biophys 38 (2009) 385–403. [PubMed: 19245337]

[21]. Tycko R, Solid-state NMR studies of amyloid fibril structure, Annu. Rev. Phys. Chem 62 (2011) 279–299. [PubMed: 21219138]

[22]. Bokvist M, Lindstrom F, Watts A, Grobner G, Two types of Alzheimer's betaamyloid (1–40) peptide membrane interactions: aggregation preventing transmembrane anchoring versus accelerated surface fibril formation, J. Mol. Biol 335 (2004) 1039–1049. [PubMed: 14698298]

[23]. Williams TL, Serpell LC, Membrane and surface interactions of Alzheimer's Abeta peptide - insights into the mechanism of cytotoxicity, FEBS J. 278 (2011) 3905–3917. [PubMed: 21722314]

[24]. Sugiura Y, Ikeda K, Nakano M, High membrane curvature enhances binding, conformational changes, and fibrillation of amyloid-beta on lipid bilayer surface, Langmuir 31 (42) (2015) 11549–11557. [PubMed: 26474149]

[25]. Qiang W, Yau WM, Schulte J, Fibrillation of beta amyloid peptides in the presence of phospholipid bilayers and the consequent membrane disruption, Biochim. Biophys. Acta Biomembr 1848 (1) (2015) 266–276.

[26]. Qiang W, Akinlolu RD, Nam M, Shu N, Structural evolution and membrane interaction of the 40-residue beta amyloid peptides: differences in the initial proximity between peptides and the membrane bilayer studied by solid-state nulear magnetic resonance spectroscopy, Biochemistry 53 (48) (2014) 7503–7514. [PubMed: 25397729]

[27]. Hellstrand E, Sparr E, Linse S, Retardation of Abeta fibril formation by phospholipid vesicles depends on membrane phase behavior, Biophys. J 98 (10) (2010) 2206–2214. [PubMed: 20483329]

[28]. Niu Z, Zhao W, Zhang Z, Xiao F, Tang X, Yang J, The molecular structure of Alzheimer b-amyloid fibrils formed in the presence of phospholipid vesicles, Angew. Chem. Int. Ed 53 (2014) 9247–9297.

[29]. Ding H, Schauerte JA, Steel DG, Gafni A, Beta-amyloid (1–40) peptide interactions with supported phospholipid membranes: a single-molecule study, Biophys. J 103 (7) (2012) 1500–1509. [PubMed: 23062342]

[30]. Delgado DA, Doherty K, Cheng Q, Kim H, Xu D, Dong H, Grewer C, Qiang W, Distinct membrane disruption pathways induced by the 40-residue beta-amyloid peptides, J. Biol. Chem 291 (23) (2016) 12233–12244. [PubMed: 27056326]

[31]. Wood WG, Eckert GP, Igbavboa U, Muller WE, Amyloid beta-protein interactions with membranes and cholesterol: causes or casualties of Alzheimer's disease, Biochim. Biophys. Acta 1610 (2) (2003) 281–290. [PubMed: 12648781]

[32]. Sciacca MF, Kotler SA, Brender JR, Chen J, Lee DK, Ramamoorthy A, Twostep mechanism of membrane disruption by Abeta through membrane fragmentation and pore formation, Biophys. J 103 (4) (2012) 702–710. [PubMed: 22947931]

[33]. Vestergaard MC, Morita M, Hamada T, Takagi M, Membrane fusion and vesicular transformation induced by Alzheimer's amyloid beta, Biochim. Biophys. Acta 1828 (4) (2013) 1314–1321. [PubMed: 23357358]

[34]. Akinlolu RD, Nam M, Qiang W, Competition between fibrillation and induction of vesicle fusion for the membrane-associated 40-residue b amyloid peptides, Biochemistry 54 (22) (2015) 3416–3419. [PubMed: 25988500]

[35]. Glabe CG, Common mechanisms of amyloid oligomer pathogenesis in degenerative disease, Neurobiol. Aging 27 (4) (2006) 570–575. [PubMed: 16481071]

[36]. Quist A, Doudevski I, Lin H, Azimova R, Ng D, Frangione B, Kagan B, Ghiso J, Lal R, Amyloid ion channels: a common structural link for protein-misfolding disease, Proc. Natl. Acad. Sci 102 (30) (2005) 10427–10432. [PubMed: 16020533]

[37]. Lal R, Lin H, Quist AP, Amyloid beta ion channel: 3D structure and relevance to amyloid channel paradigm, Biochim. Biophys. Acta 1768 (8) (2007) 1966–1975. [PubMed: 17553456]

[38]. Connelly L, Jang H, Arce FT, Ramachandran S, Kagan BL, Nussinov R, Lal R, Effects of point substitutions on the structure of toxic Alzheimer's beta-amyloid channels: atomic force microscopy and molecular dynamics simulations, Biochemistry 51 (14) (2012) 3031–3038. [PubMed: 22413858]

[39]. Capone R, Jang H, Kotler SA, Connelly L, Arce FT, Ramachandran S, Kagan BL, Nussinov R, Lal R, All-D-enantiomer of beta-amyloid peptide forms ion channels in lipid bilayers, J. Chem. Theo. Comp 8 (2012) 1143–1152.

[40]. Calderon RO, Attema B, DeVries GH, Lipid composition of neuronal cell bodies and neurites from cultured dorsal root ganglia, J. Neurochem 64 (1) (1995) 424–429. [PubMed: 7798942]

[41]. Lemkul JA, Bevan DR, Lipid composition influences the release of Alzheimer's amyloid beta-peptide from membanes, Protein Sci. 20 (9) (2011) 1530–1545. [PubMed: 21692120]

[42]. Morcombe CR, Gaponenko V, Byrd RA, Zilm KW, Diluting abundant spins by isotope edited radio frequency field assisted diffusion, J. Am. Chem. Soc 126 (23) (2004) 7196–7197. [PubMed: 15186155]

[43]. Manolikas T, Herrmann T, Meier BH, Protein structure determination from 13C spin-diffusion solid-state NMR spectroscopy, J. Am. Chem. Soc 130 (12) (2008) 3959–3966. [PubMed: 18321098]

[44]. Jaroniec CP, Tounge BA, Hertzfeld J, Griffin RG, Frequency selective heteronuclear dipolar recoupling in rotating solids: accurate 13C-15N distance measurements in uniformly 13C, 15N-labeled peptides, J. Am. Chem. Soc 123 (2001) 3507–3519. [PubMed: 11472123]

[45]. Petkova AT, Tycko R, Sensitivity enhancement in structural measurements by solid state NMR through pulsed spin locking, J. Magn. Reson 155 (2) (2004) 293–299.

[46]. Tycko R, Symmetry-based constant-time homonuclear dipolar recoupling in solid state NMR, J. Chem. Phys 126 (6) (2007) 064506. [PubMed: 17313228]

[47]. Matsuzaki K, Physicochemical interactions of amyloid beta-peptide with lipid bilayers, Biochim. Biophys. Acta Biomembr 2007 (1768) 1935–1942.

[48]. Matsuzaki K, How do membranes initiate Alzheimer's disease? Formation of toxic amyloid fibrils by the amyloid beta-protein on ganglioside clusters, Acc. Chem. Res 47 (2014) 2397–2404. [PubMed: 25029558]

[49]. Kakio A, Nishimoto S, Yanagisawa K, Kozutsumi Y, Matsizaki K, Interactions of amyloid beta-protein with various gangliosides in raft-like membranes: importance of GM1 ganglioside-bound form as an endogenous seed for Alzheimer amyloid, Biochemistry 41 (2002) 7385–7390. [PubMed: 12044171]

[50]. Kawarabayashi T, Shoji M, Younkin LH, Lin W, Dickson DW, Murakami T, Matsubara E, Abe K, Ashe KH, Younkin SG, Dimeric amyloid beta protein rapidly accumulates in lipid rafts followed by Apolipoprotein E and phosphorylated Tau accumulation in the Tg2576 mouse model of Alzheimer's disease, J. Neurosci 24 (15) (2004) 3801–3809.

[51]. Fritzsching KJ, Kim J, Holland GP, Probing lipid-cholesterol inDOPC/eSM/Chol and DOPC/DPPC/Chol model lipid rafts with DSC and 13C solid-state NMR, Biochim. Biophys. Acta 2013 (1828) 1889–1898.

[52]. Yanagisawa K, Role of gangliosides in Alzheimer's disease, Biochim. Biophys. Acta 2007 (1768) 1943–1951.

[53]. Ikeda K, Yamaguchi T, Fukunaga S, Hoshino M, Matsuzaki K, Mechanism of amyloid beta-protein aggregation mediated by GM1 ganglioside clusters, Biochemistry 50 (2011) 6433–6440. [PubMed: 21682276]

[54]. Murphy RM, Kinetics of amyloid formation and membrane interaction with amyloidogenic proteins, Biochim. Biophys. Acta 1768 (8) (2007) 1923–1934. [PubMed: 17292851]

[55]. Qiang W, Yau WM, Tycko R, Structural evolution of Iowa mutant b-amyloid fibrils from polymorphic to homogeneous states under repeated seeded growth, J. Am. Chem. Soc 133 (11) (2011) 4018–4029. [PubMed: 21355554]

[56]. Petkova AT, Yau WM, Tycko R, Experimental constraints on quaternary structure in Alzheimer's beta-amyloid fibrils, Biochemistry 45 (2) (2006) 498–512. [PubMed: 16401079]

[57]. Lu JX, Qiang W, Yau WM, Schwieters CD, Meredith SC, Tycko R, Molecular Structure of Beta-amyloid Fibrils in Alzheimer's Disease Brain Tissue, 154 (6) (2013) 1257–1248 (2013).

[58]. Paravastu AK, Leapman RD, Yau WM, Tycko R, Molecular structural basis for polymorphism in Alzheimer's beta-amyloid fibrils, Proc. Natl. Acad. Sci. U. S. A 105 (47) (2008) 18349–18354. [PubMed: 19015532]

[59]. Qiang W, Yau WM, Luo YQ, Mattson MP, Tycko R, Antiparallel beta-sheet architecture in Iowa-mutant beta-amyloid fibrils, Proc. Natl. Acad. Sci. U. S. A 109 (12) (2012) 4443–4448. [PubMed: 22403062]

[60]. Walti M, Ravotti F, Arai H, Glabe CG, Wall JS, Bockmann A, Guntert P, Meier BH, Riek R, Atomic-resolution structure of a disease-relevant Ab(1–42) amyloid fibril, Proc. Natl. Acad. Sci (2016) E4976–E4984. [PubMed: 27469165]

[61]. Colvin MT, Silvers R, Ni QZ, Can TV, Sergeyev I, Rosay M, Donovan KJ, Michael B, Wall J, Linse S, Griffin RG, Atomic resolution structure of monomorphic Ab42 amyloid fibrils, J. Am. Chem. Soc 138 (30) (2016) 9663–9674. [PubMed: 27355699]

[62]. Reitz C, Alzheimer's disease and the amyloid cascade hypothesis: a critical review, Int. J. Alzheimers Dis. 2012 (2012) 369808. [PubMed: 22506132]

[63]. Korshavn KJ, Bhunia A, Lim MH, Ramamoorthy A, Amyloid-beta adopts a conserved, partially folded structure upon binding to zwitterionic lipid bilayers prior to amyloid formation, Chem. Commun 52 (2016) 882–885.

[64]. Kotler SA, Walsh P, Brender JR, Ramamoorthy A, Differences between amyloidb-aggregation in solution and on the membrane: insights into elucidation of the mechanistic details of Alzheimer's disease, Chem. Soc. Rev 43 (2014) 6692. [PubMed: 24464312]

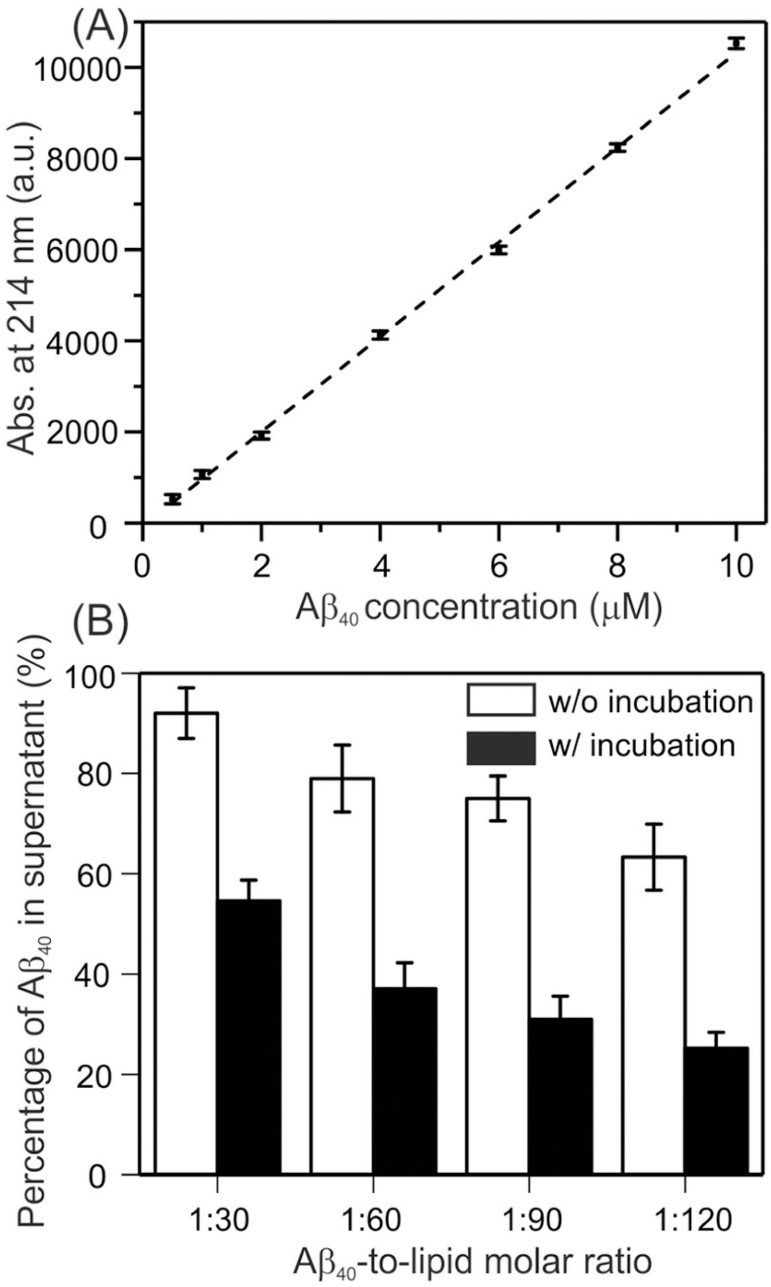

Fig. 1.

Quantification of the Aβ40-membrane binding using analytical HPLC. (A) Standard curve to show the linear relationship between the concentration of freshly dissolved Aβ40 and peak areas at 214 nm. (B) Quantification of Aβ40 in supernatants (reported as the percentage of initial Aβ40) in biological membrane mimics at time zero (open bars) and after 4 h of incubation (solid bars). Error bars were determined from three independent measurements.

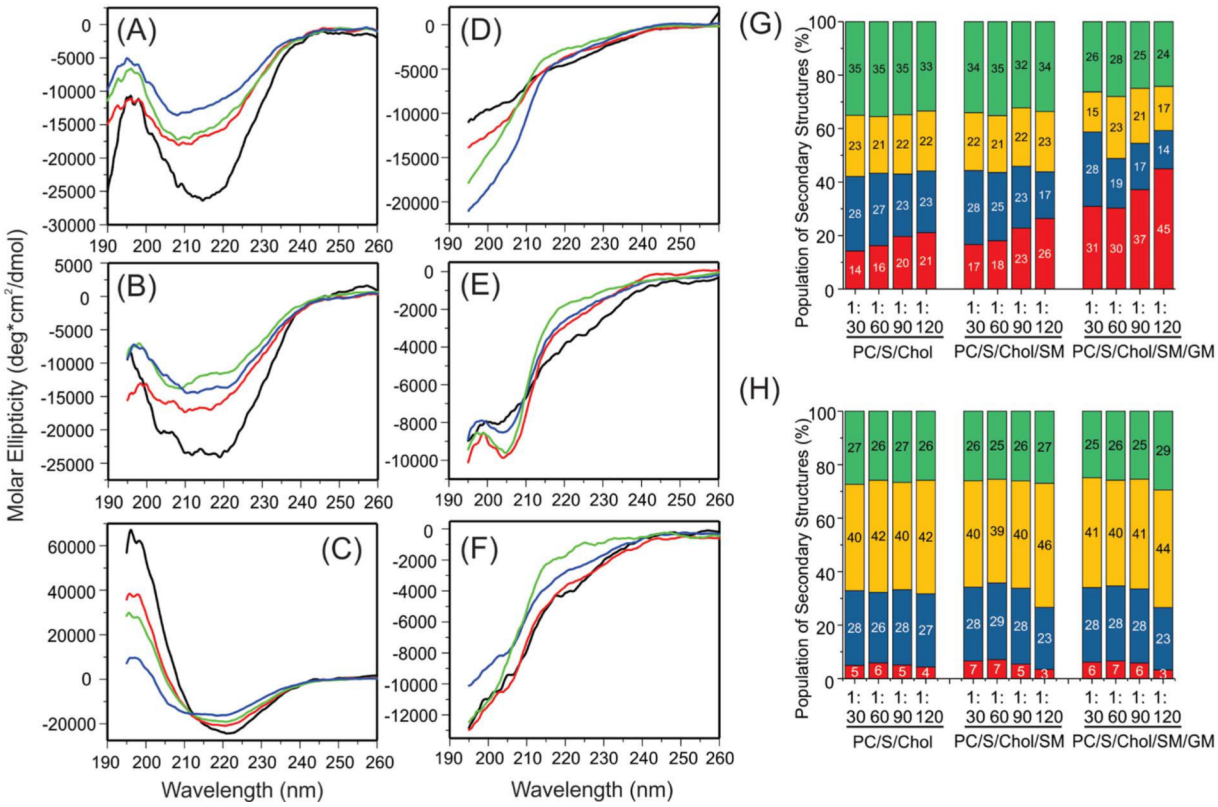

Fig. 2.

CD spectra and analysis of secondary structures. (A–F) CD spectra for (A and D) DMPC/PS/Cholesterol, (B and E) DMPC/PS/Cholesterol/sphingomyelin, and (C and F) DMPC/PS/ Cholesterol/sphingomyelin/ganglioside GM1 before (A–C) and after (D–F) incubation. Samples with different Aβ40-to-lipid ratios were shown in colors: black, 1:30; red, 1:60; green, 1:90; and blue, 1:120. (G–H) Analysis of secondary structures from the CD spectra before (panel G) and after (panel H) incubation. Colors show different types of secondary structures: red, α-helix; blue, β-strand; yellow, β-turn; and green, random coil.

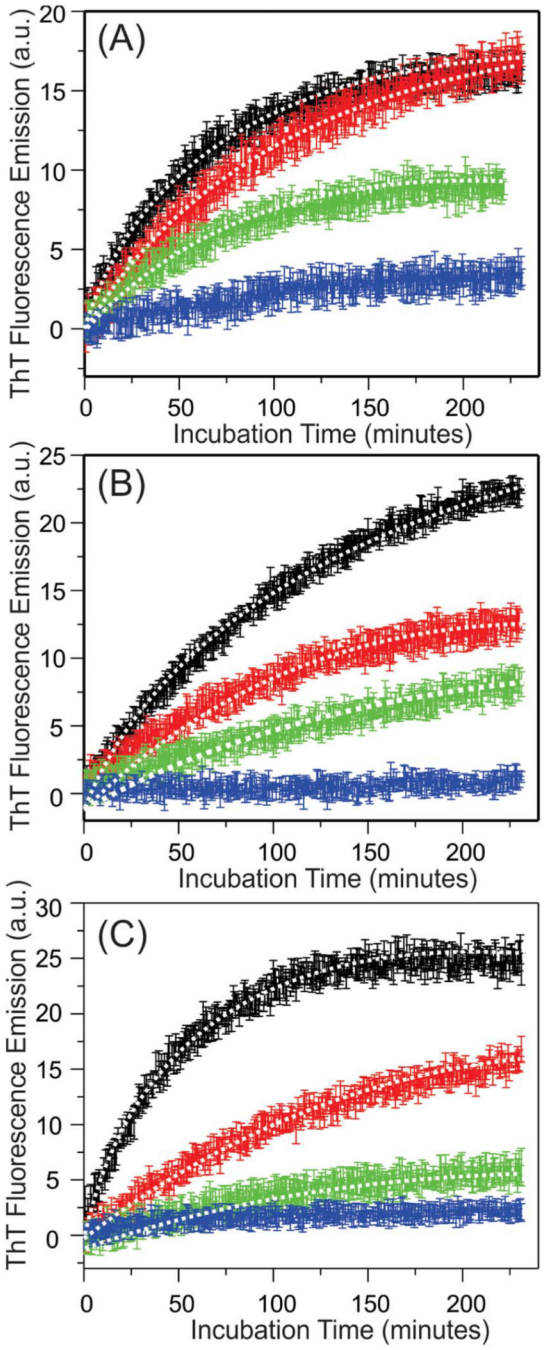

Fig. 3.

Plots of the kinetics of ThT fluorescence for (A) DMPC/PS/Cholesterol, (B) DMPC/ PS/ Cholesterol/sphingomyelin, and (C) DMPC/PS/Cholesterol/sphingomyelin/ganglioside GM1 samples. The samples with Aβ40-to-lipid ratios 1:30, 1:60, 1:90 and 1:120 are shown in black, red, green and blue respectively. For individual data points, the error bars were obtained from three independent measurements. The best-fit curves were shown by dashed lines along with the corresponding experimental traces.

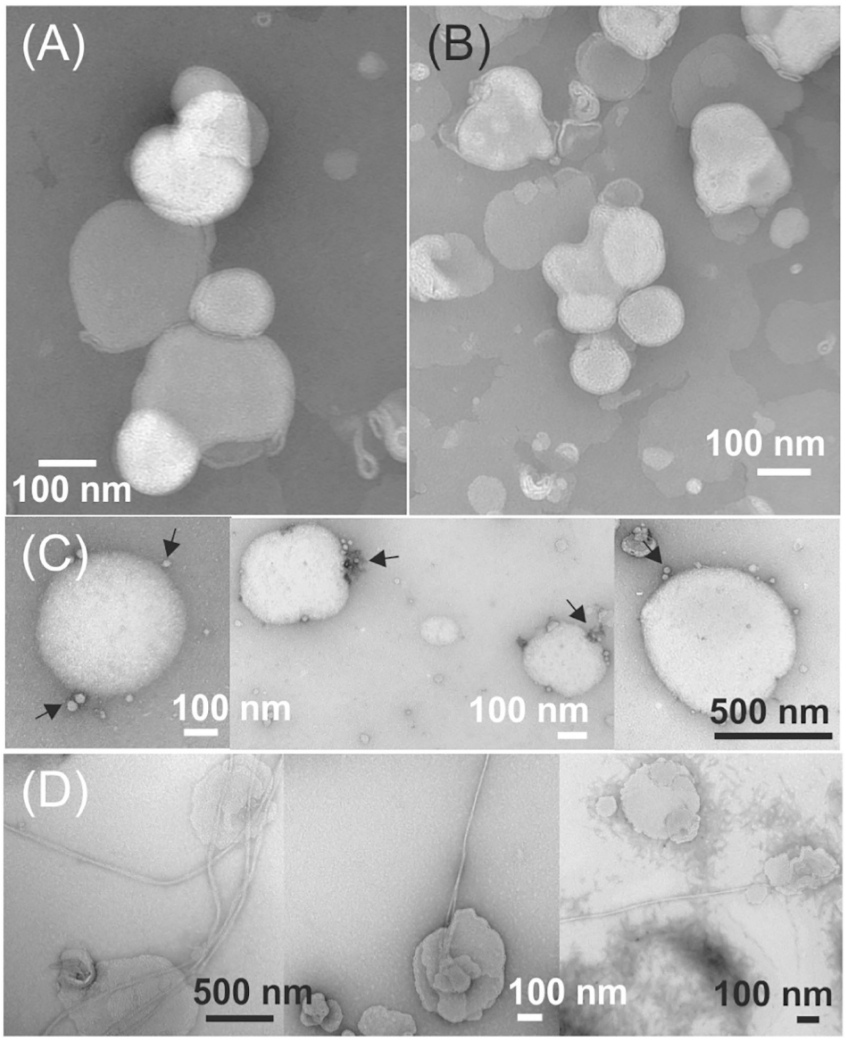

Fig. 4.

Negatively stained TEM images of DMPC/PS/Cholesterol/sphingomyelin/ganglioside GM1 samples with (A) 1:120 ratio and 4-hour incubation time, (B) 1:30 ratio and 4-hour incubation time, (C) 1:120 ratio and 48-hour incubation time, and (D) 1:30 ratio and 48-hour incubation time. The arrows in panel (C) indicate the small spherical aggregates on membrane surfaces.

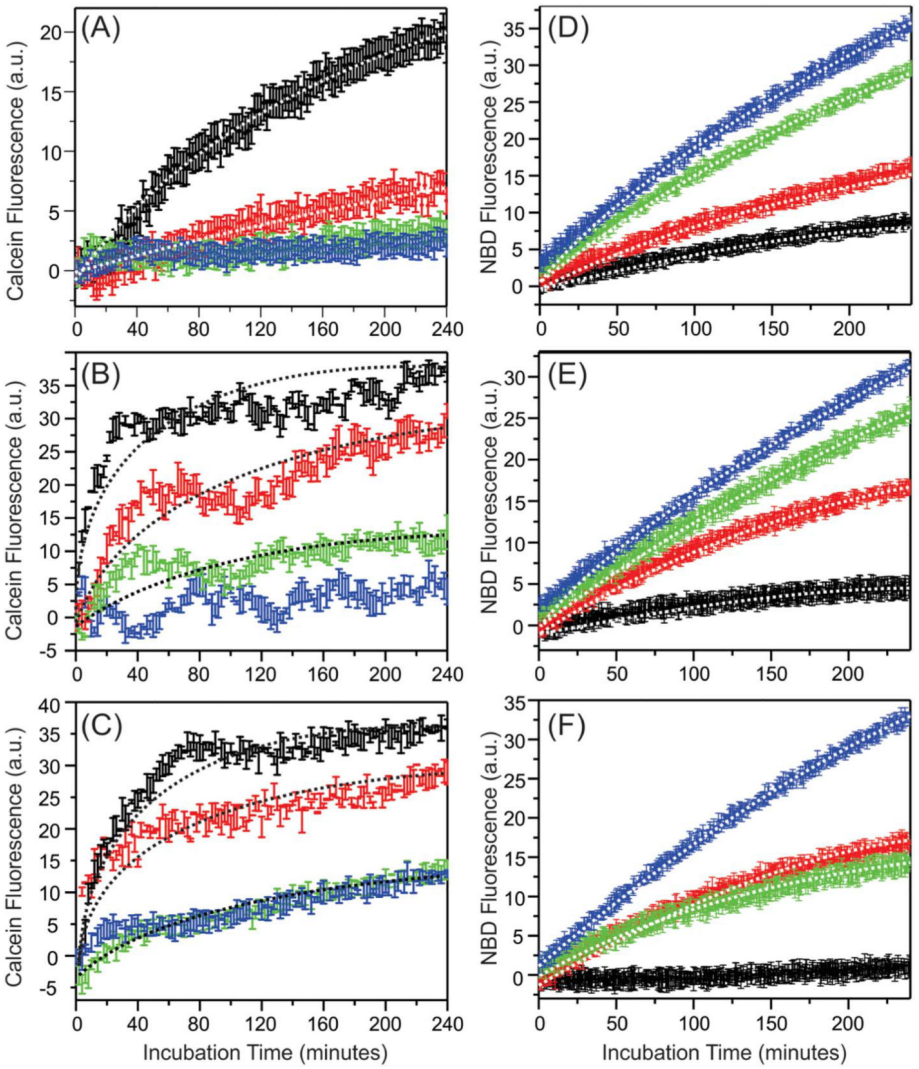

Fig. 5.

Plots of kinetic curves of (A–C) calcein membrane leakage and (D–F) lipid mixing measurements for (A and D) DMPC/PS/Cholesterol, (B and E) DMPC/PS/Cholesterol/sphingomyelin, and (C and F) DMPC/PS/Cholesterol/sphingomyelin/ganglioside GM1 samples. The samples with Aβ40-to-lipid ratios 1:30, 1:60, 1:90 and 1:120 are shown in black, red, green and blue respectively. For individual data points, the error bars were obtained from three independent measurements. The best-fit curves were shown by dashed lines along with the corresponding experimental traces.

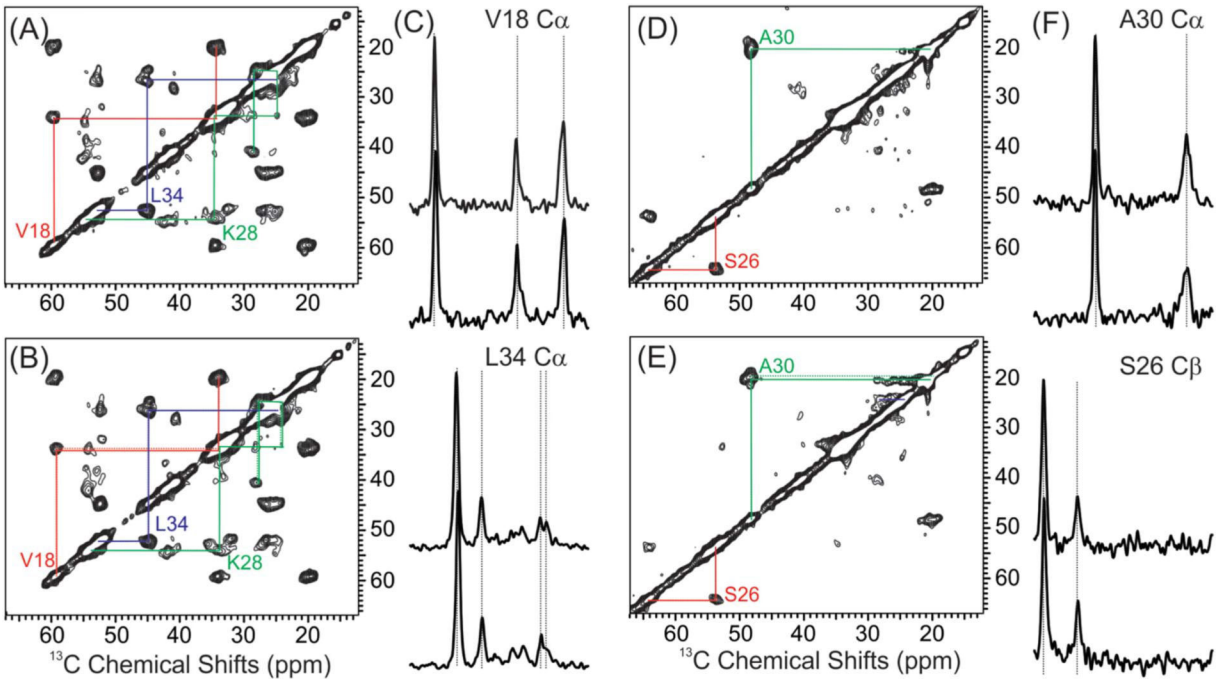

Fig. 6.

Representative 2D ^{13}C-^{13}C spin diffusion ssNMR spectra and 1D slices. (A–B) 2D spectra of samples labeled at V18, F20, D23, K28, G29 and L34 with POPC (panel A) and DMPC/PS/cholesterol/sphingomyelin/ganglioside GM1 (panel B) membranes. Intra-residue cross peaks for individual residues are highlighted using colored lines. (C) Representative 1D slices along the V18 Cα and L34 Cα in indirect dimension. Comparison of ^{13}C peaks are highlighted with dashed lines to show little changes in different samples. (D–F) 2D and 1D spectra for samples labeled at S26 and A30. The 1D slices shown are along the ^{13}C chemical shifts of A30 Cα and S26 Cβ.

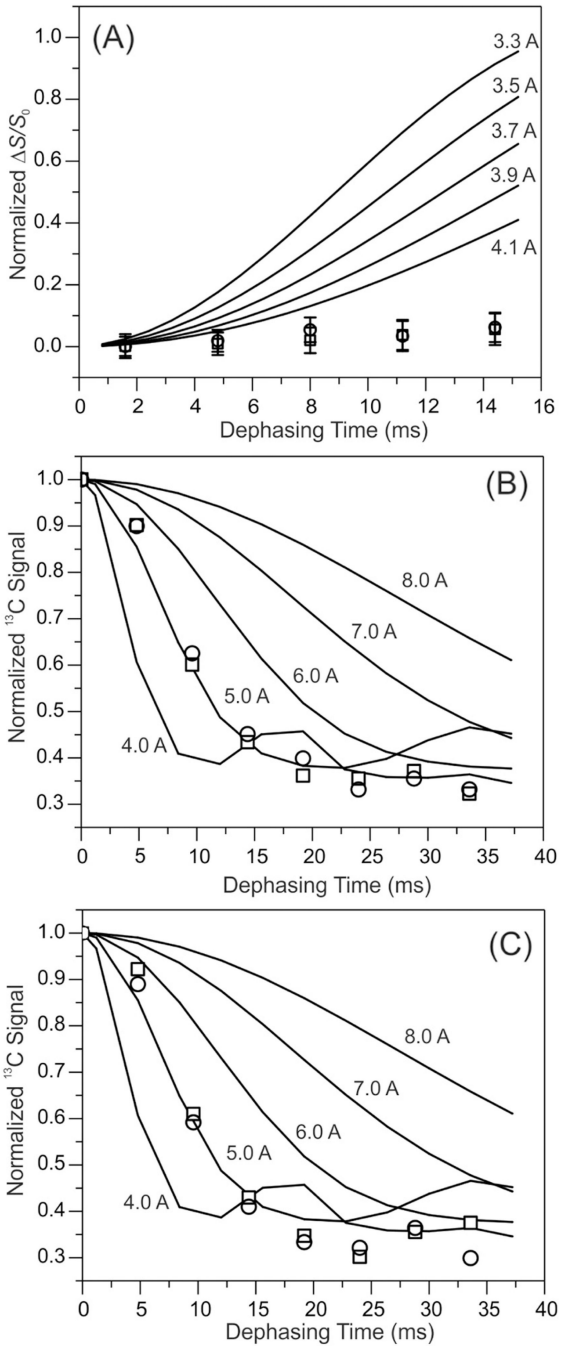

Fig. 7.

(A) The plots of ^{15}N-^{13}C fsREDOR dephasing versus dipolar evolution times for fibrils grown with POPC (squares) and DMPC/PS/Cholesterol/sphingomyelin/ganglioside GM1 (circles) membranes. Simulation curves for ^{15}N-^{13}C distances 3.3–4.1 Å were shown in solid lines. The results confirmed the absence of D23 Cγ-K28 Nε salt bridge in either fibril structure. (B-C) Plots of 13C-PITHIRDs dephasing curves for the C′ of V18 (panel B) and M35 (panel C). Similar to Panel (A), open squares and circles show the data in POPC and DMPC/PS/Cholesterol/sphingomyelin/ganglioside GM1 membranes respectively.

Simulation curves for 4–8 Å distances are shown. The uncertainties for individual measurements were ~ 0.05 for all data.

Table 1

Fitting of ThT kinetics.

Membrane composition	$A\beta_{40}$-to-lipid ratio	k (min^{-1})	$I_0 + I_1$ (a.u.)
DMPC/DMPS/cholesterol	1:30	0.0159 (0.0011)	16.71 (3.05)
	1:60	0.0073 (0.0008)	19.28 (3.07)
	1:90	0.0072 (0.0007)	7.23 (2.98)
	1:120	_[a]	–
DMPC/DMPS/cholesterol/sphingomyelin	1:30	0.0078 (0.0008)	26.98 (3.11)
	1:60	0.0081 (0.0008)	14.92 (3.03)
	1:90	0.0027 (0.0005)	16.86 (3.08)
	1:120	–	–
DMPC/DMPS/cholesterol/sphingomyelin/ganglioside GM1	1:30	0.0206 (0.0012)	25.36 (2.77)
	1:60	0.0073 (0.0008)	18.27 (2.91)
	1:90	0.0070 (0.0007)	7.98 (2.56)
	1:120	–	–

[a]The increment of fluorescence was insignificant.

Table 2

Fitting of the calcein leakage kinetics.

Membrane composition	$A\beta_{40}$-to-lipid ratio	k (min^{-1})	% of leakage[a]
DMPC/DMPS/cholesterol	1:30	0.0203 (0.0022)	22.42 (4.19)
	1:60	0.0049 (0.0023)	18.15 (4.23)
	1:90	_[b]	–
	1:120	–	–
DMPC/DMPS/cholesterol/sphingomyelin	1:30	0.2276 (0.0045)	25.33 (3.92)
	1:60	0.0671 (0.0039)	18.00 (4.03)
	1:90	0.0055 (0.0038)	6.54 (4.11)
	1:120	–	–
DMPC/DMPS/cholesterol/sphingomyelin/ganglioside GM1	1:30	0.1414 (0.0031)	29.02 (3.73)
	1:60	0.0550 (0.0033)	18.85 (3.32)
	1:90	0.0067 (0.0037)	12.86 (3.94)
	1:120	0.0065 (0.0035)	12.77 (4.01)

[a] Percentage of leakage was calculated as $(I_0 + I_1)/I_{max}$.

[b] The increment of fluorescence was insignificant.

Table 3

Fitting of the lipid mixing kinetics.

Membrane composition	$A\beta_{40}$-to-lipid ratio	k (min^{-1})	% of lipid mixing[a]
DMPC/DMPS/cholesterol	1:30	0.0028 (0.0004)	20.55 (3.22)
	1:60	0.0023 (0.0003)	47.12 (2.05)
	1:90	0.0023 (0.0003)	90.94 (2.07)
	1:120	0.0022 (0.0003)	88.70 (2.21)
DMPC/DMPS/cholesterol/sphingomyelin	1:30	0.0060 (0.0005)	4.32 (2.29)
	1:60	0.0051 (0.0003)	16.48 (3.03)
	1:90	0.0014 (0.0003)	61.87 (2.61)
	1:120	0.0014 (0.0003)	66.76 (3.12)
DMPC/DMPS/cholesterol/sphingomyelin/ganglioside GM1	1:30	_[b]	–
	1:60	0.0046 (0.0003)	16.09 (2.22)
	1:90	0.0059 (0.0004)	17.06 (2.47)
	1:120	0.0024 (0.0003)	52.19 (3.05)

[a] Percentage of leakage was calculated as $(I_0 + I_1)/I_{max}$.

[b] The increment of fluorescence was insignificant.

Table 4

^{13}C chemical shifts of fibrils grown with different membrane compositions.

POPC							DMPC/S/Cholesterol/sphingomyelin/ganglioside GM1						
	C′ ppm	Cα ppm	Cβ ppm	Cγ ppm	Cδ ppm	Ce ppm		C′ ppm	Cα ppm	Cβ ppm	Cγ ppm	Cδ ppm	Ce ppm
L17	172.8	52.2	43.1	26.3	24.8		L17	173.1	52.2	43.5	26.6	24.2	
V18	171.7	60.0	34.4	20.6			V18	171.6	59.4	34.2	20.4		
				19.8							19.5		
F20	171.0	54.7	41.7				F20	170.6	54.5	42.2			
D23	173.2	52.5	41.3	175.6			D23	–	–	–	–		
S26	172.2	53.9	64.1				S26	172.2	53.8	64.2			
N27	170.7	51.2	38.8	174.7			N27	172.2	51.4	38.9	174.7		
K28	173.9	54.2	34.5	25.4	28.4	41.2	K28	174.1	54.2	34.3	24.8	28.1	40.9
G29	170.6	42.3					G29	170.4	42.3				
A30	173.8	48.6	20.7				A30	173.5	48.5	20.8			
I32	174.5	56.2	40.7	25.4	15.3		I32	174.4	56.2	41.0	25.4	15.6	
					12.6							12.5	
G33	170.3	47.6					G33	170.4	47.8				
L34	172.5	52.6	45.0	26.7	24.8		L34	172.6	52.5	44.8	26.6	24.4	
G38	169.1	43.2					G38	169.5	43.5				
V39	–	58.8	33.7	20.7			V39	–	59.2	33.8	20.0		